Available online at www.sciencedirect.com
ScienceDirect
Journal of Power Sources 161 (2006) 19–26
JOURNAL OF POWER SOURCES
www.elsevier.com/locate/jpowsour

Effect of sulfur and nickel doping on morphology and electrochemical performance of $LiNi_{0.5}Mn_{1.5}O_{4-x}S_x$ spinel material in 3-V region

Yang-Kook Sun [a,*], Sung Woo Oh [a], Chong Seung Yoon [a], Hyun Joo Bang [b], Jai Prakash [b]

[a] *Center for Information and Communication Materials, Department of Chemical Engineering, Hanyang University, 133-791 Seoul, Republic of Korea*
[b] *Center for Electrochemical Science and Engineering, Department of Chemical and Environmental Engineering, Illinois Institute of Technology, 10 W. 33rd Street, Chicago, IL, USA*

Received 10 January 2006; accepted 20 March 2006
Available online 6 June 2006

Abstract

The effect of nickel and sulfur substitution for manganese and oxygen on the structure and electrochemical properties of the $LiNi_{0.5}Mn_{1.5}O_{4-x}S_x$ is examined. The $LiNi_{0.5}Mn_{1.5}O_{4-x}S_x$ ($x=0$ and 0.05) compounds are successfully synthesized at 500 and 800 °C by co-precipitation using the metal carbonate $(Ni_{0.5}Mn_{1.5})CO_3$ as a precursor. The resulting powder with sulfur doping exhibits different morphology from a Ni-only doped spinel in terms of particle size and surface texture. The $LiNi_{0.5}Mn_{1.5}O_{4-x}S_x$ ($x=0$ and 0.05) powders are characterized by X-ray diffraction (XRD), scanning electron microscopy (SEM), and galvanostatic charge–discharge cycling. The nickel- and sulfur-doped spinel displays excellent capacity retention and rate capability in the 3-V region, compared with Ni-only doped spinel material.

Keywords: Li-ion battery; 3-V spinel; Sulfur and nickel doping; Cathode; Capacity retention; Rate capability

1. Introduction

Manganese spinel and its derivatives have been studied extensively because of their cost advantages and environmentally friendliness as cathode materials for Li-ion batteries. Nevertheless, commercialization of these materials in Li-ion batteries has been delayed due to poor cycling performance at room temperature as well as at elevated temperatures [1–4]. Several efforts have been made to overcome this critical problem and to understand the mechanism of the observed rapid capacity fading [2–6]. Partial cation doping of manganese in the host structure by various components (Cr, Al, Ni, Co, Fe, etc.) has yielded successful improvements and have also revealed that one of the main mechanisms of capacity fading is related to dissolution of Mn^{2+} ions through a disproportionation reaction in the presence of HF in the electrolyte [5–12]. Partial cation substitution results in a smaller reversible capacity because of the reduced amount of Mn^{3+} as a redox ion in the 4-V range of $Li_xMn_2O_4$.

Other approaches to suppress capacity fading in the 3-V region involve the anion (e.g., sulfur) doping for oxygen in the spinel structure [10]. It has been suggested [13] that spinel suffers capacity fading primarily because of Jahn-Teller distortion due to the existence of high spin Mn^{3+} in the 3-V range. It is proposed that this effect occurs when the oxidation state of Mn approaches exactly 3.5 (Mn^{3+}/Mn^{4+}; 1:1), which is associated with unstable structural integrity caused by a large change (16%) in lattice constant [13,14]. It has been claimed [14] that the spinel oxide experiences a structural change from cubic to tetragonal accompanied by a lattice volume change as the concentration gradient on the surface/bulk of the spinel reaches more than 1.0 due to slow diffusion of Li ions. $Li_xMn_2O_4$ ($0<x<1$) exhibits capacity in the 3-V region when excess Li ions are inserted into the structure (16d octahedral site instead of 8a tetrahedral site) to result in the formula of $Li_{1+x}Mn_2O_4$ ($1<x<2$) with Mn ions in an oxidation state below +3.5. The structural distortion is too large to maintain the host framework during lithium insertion–extraction. The crystal structure changes from cubic ($c/a=1$) to tetragonal symmetry ($c/a=1.16$) [14]. Therefore, capacity fading in the 3-V range for the spinel has been shown to be more significant than that of spinel in the 4-V range [13–16].

* Corresponding author. Tel.: +82 2 2220 0524; fax: +82 2 2282 7329.
E-mail address: yksun@hanyang.ac.kr (Y.-K. Sun).

0378-7753/$ – see front matter © 2006 Elsevier B.V. All rights reserved.
doi:10.1016/j.jpowsour.2006.03.085

Recently, $LiNi_{0.5}Mn_{1.5}O_4$ has received great deal of attention because of its high potential plateau at 4.7 V [17–20]. The application of Li-ion batteries above 4.5 V is not desirable because of the instability of present electrolytes. One of the interesting features of the spinel doped with 0.5 mol of Ni per unit formula is that the redox species in the host structure is not the manganese ion but the nickel ion (Ni^{2+} to Ni^{4+} reversibly). Consequently, Ni-doped spinel exhibits capacity at higher potential and also good capacity retention compared with $Li_xMn_2O_4$ [9,18]. Despite partial success in improving the cycling performance of the spinels at room temperature, the modified spinels still suffer from capacity fading at elevated temperatures (above 55 °C). Thus, it is considered that an understanding of the mechanism of capacity fading in the 3-V region will be helpful in improving the cycling performance of spinels at elevated temperatures and thereby allow their use as cathodes in new applications with practical capacities. This study reports the synthesis of the nickel- and sulfur-doped spinel, $LiNi_{0.5}Mn_{1.5}O_{3.95}S_{0.05}$, by a carbonate co-precipitation method and its electrochemical performance in the 3-V region.

2. Experimental

2.1. Synthesis and characterization

$LiNi_{0.5}Mn_{1.5}O_{4-x}S_x$ ($x = 0$ and 0.05) powders were synthesized by using a carbonate metal precursor (Ni-Mn)CO_3, as the starting material. The precursor is very effective in producing powders with a small particle size because during the co-precipitation process the precursor does not form large clusters as is the case when using a typical sol–gel process with metal acetate or metal nitrate hydrate precursors [21,22]. Spherical $(Ni_{0.5}Mn_{1.5})CO_3$ was prepared as follows. An aqueous solution of $NiSO_4$ and $MnSO_4$ (Ni:Mn = 1:3) with a concentration of 2.0 mol dm^{-3} was pumped into a continuously stirred tank reactor (CSTR, capacity 4L) under a CO_2 atmosphere. At the same time, a 2 M Na_2CO_3 solution together with the required amount of NH_4OH solution as a chelating agent were also separately fed into the reactor. In the initial stage of the co-precipitation reaction, irregular secondary particles of (Ni-Mn)CO_3 where formed via agglomeration of the acicular primary structure. These particles gradually assumed a spherical shape during vigorous stirring at 60 °C for 12 h. The spherical particles were filtered, washed, dried at 110 °C, and subjected to calcination at 500 °C for 5 h. The resulting powder was mixed with lithium sources ($LiOH{\cdot}H_2O$) and sulfur powder for doping, followed by final calcination at 500 and 800 °C in a box furnace.

The phase identification of the prepared powder was carried out by means of powder X-ray diffraction (XRD) using Cu Kα radiation (Rigaku, Rint-2000). Rietveld refinement was performed on the data to obtain the lattice constant. The chemical compositions of the prepared powders were analyzed by atomic absorption spectroscopy (AAS, Vario 6, Analytic Jena, Germany). Particle morphology was examined with a field emission scanning electron microscope (FESEM, Hitachi Co., S-4100). Transmission electron microscopy (TEM) images were obtained with a side-entry type high-resolution microscope (H-9000NAR) that operated at 300 kV with a point resolution of 0.18 nm.

2.2. Electrochemical evaluation

The electrochemical properties of the $LiNi_{0.5}Mn_{1.5}O_{4-x}S_x$ ($x = 0$ and 0.05) samples were evaluated using coin-type cells (size 2032) that each used a lithium metal foil as an anode, a Celgard 3401 microporous polypropylene separator, and an electrolyte containing 1.0 M $LiPF_6$ dissolved in a 1:1 vol.% mixture of ethylene carbonate (EC) and diethyl carbonate (DEC). The cathodes were fabricated using the sample powders (80 wt.%). Super P carbon black (10 wt.%) (Aldrich Chemical), and polyvinylidene fluoride (PVDF) binder (10 wt.%). The three components were added to *N*-methyl-2-pyrrolidone (NMP) and were ground to produce a homogeneous mixture. An excess amount of NMP was then added until the mixture reached the required viscosity. The mixture was then spread on an aluminum with a doctor blade, to produce a film with a thickness of 200 μm, and then was dried at 110 °C. Fabrication of the coin cells was carried out in an argon-filled glove box. The cells were cycled glavanostatically at 0.2 mA cm^{-2} over a potential range of 2.4–3.5 V for both $LiNi_{0.5}Mn_{1.5}O_4$ and $LiNi_{0.5}Mn_{1.5}O_{3.95}S_{0.05}$.

3. Results and discussion

X-ray powder diffraction patterns are shown in Fig. 1 for $LiNi_{0.5}Mn_{1.5}O_4$ and $LiNi_{0.5}Mn_{1.5}O_{3.95}S_{0.05}$ prepared at 500 °C. The patterns for both powders are representative of well-defined spinel structures with lattice parameters of $a = 8.1799$ and 8.1824 Å, respectively. The full width at half magnitude (FWHM) of all peaks for each sample indicate that the powders have a fine particle size, which is due to the low temperature of calcination and the relatively short time taken for final firing. $LiNi_{0.5}Mn_{1.5}O_4$ (no sulfur substitution) displays peaks from impurities at around $2\theta = 15$, 33 and 55°. This single-phase compound is hard to obtain in a pure state because of the formation of NiO and $Li_{0.2}Ni_{0.8}O$ that result from Ni deficiency at high temperature [7,18]. A NiO peak is not, however, detected in

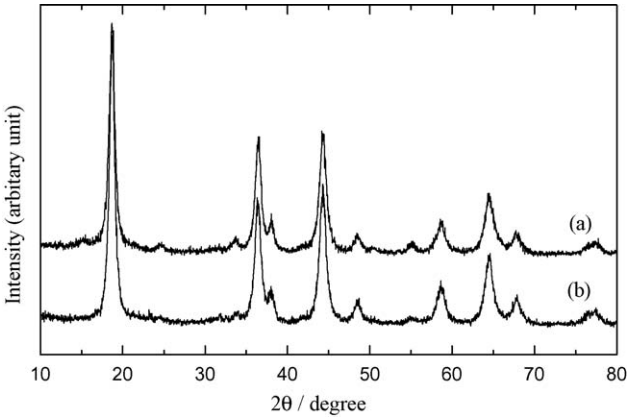

Fig. 1. X-ray powder diffraction patterns of $LiNi_{0.5}Mn_{1.5}O_{4-x}S_x$ ($x = 0$ and 0.05) prepared at 500 °C for 5 h.

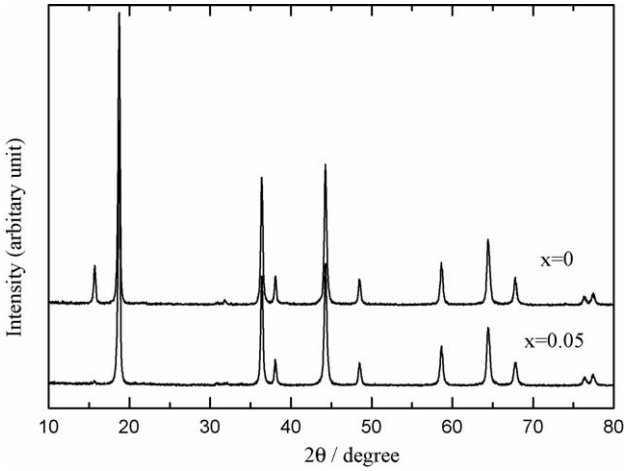

Fig. 2. X-ray powder diffraction patterns of $LiNi_{0.5}Mn_{1.5}O_{4-x}S_x$ ($x=0$ and 0.05) prepared at 800 °C for 5 h.

either of the samples prepared in the study. It is possible that the doped ions can substitute Li ions at the tetrahedral sites instead of Mn ions at octahedral sites because of the existence of $NiMn_2O_4$. It has been reported [23] that the (2 2 0) peak at 30.7° is sensitive to the position of Mn. The (2 2 0) peak should be observed if Ni ions replace Li ions at the tetrahedral sites. The absence of the (2 2 0) peak in the XRD patterns for both Ni-doped $LiNi_{0.5}Mn_{1.5}O_{4-x}S_x$ ($x=0$ and 0.05) samples indicates that doped Ni ions are located at 16d octahedral sites as are Mn ions in $Li_xMn_2O_4$.

On raising the calcination temperature, the crystallinity of both samples increases, as shown in Fig. 2. The impurity ($2\theta=15°$) detected in $LiNi_{0.5}Mn_{1.5}O_4$, prepared at 500 °C is still observed in the sample prepared 800 °C. This peak was not, however, present in the XRD pattern for the sulfur-doped sample prepared at 500 and 800 °C. The identity and origin of the peak have still to be determined. Values of the lattice constant (a) of the unit cell of the spinels with and without sulfur doping are listed in Table 1. The lattice parameter of $LiNi_{0.5}Mn_{1.5}O_{3.95}S_{0.05}$ is slightly larger than that of $LiNi_{0.5}Mn_{1.5}O_4$. This is due to the different ionic radii of S (1.70 Å) and O (1.26 Å) [24]. Also, the lattice parameter for each sample is smaller than that reported for $Li_xMn_2O_4$ because the Mn^{3+} ions have ionic radii than the Mn^{4+} ions present in $Li_xMn_2O_4$. Similarly, Amatucci and Tarascon [3] have reported that the lattice parameter for anion (F)-doped spinel increases as the amount of doped anion is increased because substitution of divalent O^{-2} with monovalent F^{-1} increases the amount of Mn^{3+}. The samples prepared

Table 1
Lattice parameters of $LiNi_{0.5}Mn_{1.5}O_{3.95}S_{0.05}$ ($x=0$ and 0.05) prepared at 500 and 800 °C

Composition	a (Å)	Volume (Å^3)	Firing temperature (°C)
$LiNi_{0.5}Mn_{1.5}O_4$	8.1799	547.323	500
$LiNi_{0.5}Mn_{1.5}O_{3.95}S_{0.05}$	8.1824	547.825	500
$LiNi_{0.5}Mn_{1.5}O_4$	8.1784	547.022	800
$LiNi_{0.5}Mn_{1.5}O_{3.95}S_{0.05}$	8.1797	547.283	800

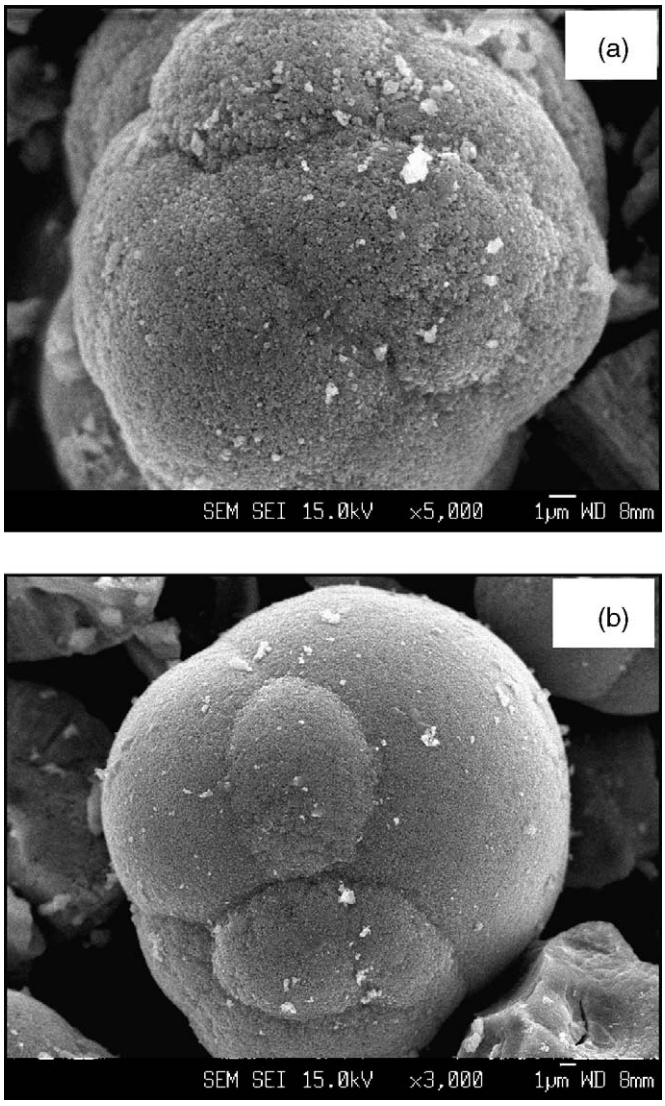

Fig. 3. Scanning electron micrograph of: (a) $LiNi_{0.5}Mn_{1.5}O_4$ prepared at 800 °C for 5 h (×5000); (b) $LiNi_{0.5}Mn_{1.5}O_{3.95}S_{0.05}$ at 800 °C for 5 h (×3000).

at 800 °C show a similar trend, i.e., $LiNi_{0.5}Mn_{1.5}O_{3.95}S_{0.05}$ has a larger lattice constant (8.1797 Å) than that of $LiNi_{0.5}Mn_{1.5}O_4$ (8.1784 Å).

Scanning electron micrographs for $LiNi_{0.5}Mn_{1.5}O_4$ and $LiNi_{0.5}Mn_{1.5}O_{3.95}S_{0.05}$ prepared at 800 °C are presented in Fig. 3. Both samples consist of spherical particles that can be distinguished by a clear difference in the surface morphology, namely, compared with $LiNi_{0.5}Mn_{1.5}O_4$, $LiNi_{0.5}Mn_{1.5}O_{3.95}S_{0.05}$ has a very smooth surface. In order to evaluate the effect of calcination temperature on surface morphology, micrographs were also recorded for samples heated at 900 °C. The particles from both samples still maintain a spherical shape (Fig. 4). A magnified view of $LiNi_{0.5}Mn_{1.5}O_4$ (Fig. 4(b)) shows that the secondary particles consist of primary particles with a size of about 0.1 μm. By contrast, the sulfur-doped sample ($LiNi_{0.5}Mn_{1.5}O_{3.95}S_{0.05}$) prepared at 900 °C has a very smooth surface, i.e., the primary particles are too small to be observed by SEM.

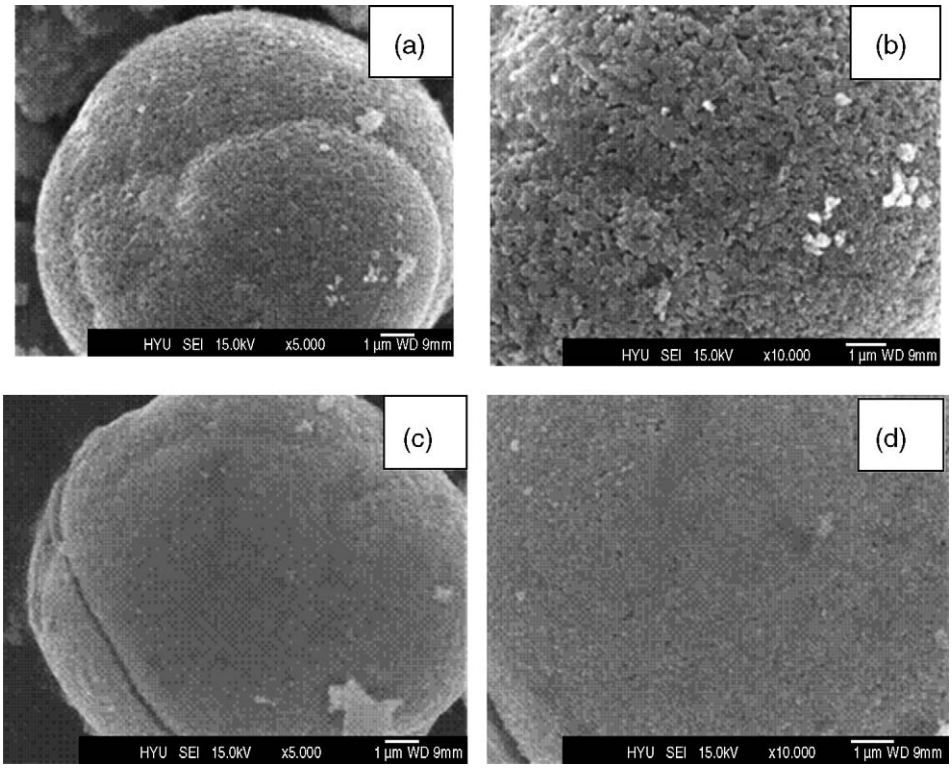

Fig. 4. Scanning electron micrograph of: (a) $LiNi_{0.5}Mn_{1.5}O_4$ prepared at 900 °C for 20 h (×5000); (b) magnified $LiNi_{0.5}Mn_{1.5}O_4$ at 900 °C for 20 h (×10,000); (c) $LiNi_{0.5}Mn_{1.5}O_{3.95}S_{0.05}$ at 900 °C for 20 h (×5000); (d) magnified $LiNi_{0.5}Mn_{1.5}O_{3.95}S_{0.05}$ at 900 °C for 20 h (×10,000).

To evaluate the effect of sulfur doping on the morphology of $LiNi_{0.5}Mn_{1.5}O_4$, transmission electron micrographs were taken for both the no-sulfur and the sulfur-doped spinel samples. It is found that $LiNi_{0.5}Mn_{1.5}O_{3.95}S_{0.05}$ prepared at 500 °C is comprised of nanometer-sized primary particles (Fig. 5) that could not be detected in the SEM image (Fig. 3(b)), as described above. The primary particles have ill-defined shapes (Fig. 5(a)) with diameters of ∼10 nm, as can be seen embedded in the circle highlighted in Fig. 5(b). The micrograph clearly indicates that each particle consists of an agglomerate of loosely held, nano-scale crystals. The edge of the particles cannot be clearly distinguished, which suggests that the particle surface is quite rough and that these primary particles are held together by mechanical means rather than by a chemical binding force. Such a loose structure would better accommodate any volume changes associated with structural transition or Li insertion [21].

A magnified TEM image of sulfur-free $LiNi_{0.5}Mn_{1.5}O_4$ particles prepared at 500 °C is given in Fig. 6. The primary particles of sulfur-free powders are also extremely small (∼10 nm in diameter), similar to those in the sulfur-doped sample. In this sample, however, large elongated particles (∼50 nm long) are interspersed among much smaller particles (indicated by the arrow).

Transmission electron micrographs for both samples prepared at 800 °C are shown in Fig. 7. The primary particles have grown substantially larger due to coarsening. Although it is difficult to estimate the average particle size from the micrographs, it appears that the primary particles of sulfur-doped spinel ($LiNi_{0.5}Mn_{1.5}O_{3.95}S_{0.05}$) tend to be smaller than those of the sulfur-free sample ($LiNi_{0.5}Mn_{1.5}O_4$). The primary particles of the sulfur-free sample had polygonal shapes due to faceting, whereas those of the sulfur-doped sample ($LiNi_{0.5}Mn_{1.5}O_{3.95}S_{0.05}$) have an irregular shape with rough edges. The two primary particles indicated by arrows in Fig. 7 exemplify the morphological differences between the two samples. In contrast to the smooth surface observed at a microscopic scale by SEM, the surface of each primary particle in the sulfur-doped powder is quite rough at the nanometer scale. In summary, therefore, sulfur doping reduces the primary particles size while narrowing the size distribution, and also suppresses faceting during growth that results in the formation of irregular-shaped particles with a rough surface structure.

Discharge–charge curves are given in Fig. 8 for a $LiNi_{0.5}Mn_{1.5}O_{4-x}S_x$ ($x=0$ and 0.05) electrode (prepared at 500 °C) in a voltage range of 2.4–3.5 V at a current density of 0.2 mA cm^{-2}. Both electrodes display a flat voltage profile, that is located at an average potential of 2.85 V (average potential from discharge and charge curves). The voltage profile is slightly lower than that reported for $LiMn_2O_4$, viz., 2.95 V [2,17]. With cycling, the capacity for both electrodes becomes stabilized without any rapid capacity loss. The delivered capacities are 121 and 102 mA h g^{-1} for $LiNi_{0.5}Mn_{1.5}O_{3.95}S_{0.05}$ and $LiNi_{0.5}Mn_{1.5}O_4$, respectively. The capacity in the 3-V range is attributed to insertion–extraction of lithium into the 16d site, instead of the 8a site. Ohzuku et al. [25] concluded that the 3-V capacity originates from the conversion of the $LiNi_{0.5}Mn_{1.5}O_4$ to $Li_2Ni_{0.5}Mn_{1.5}O_4$, which consists of two-phase reaction (cubic–tetragonal) as in $Li_1Mn_2O_4$.

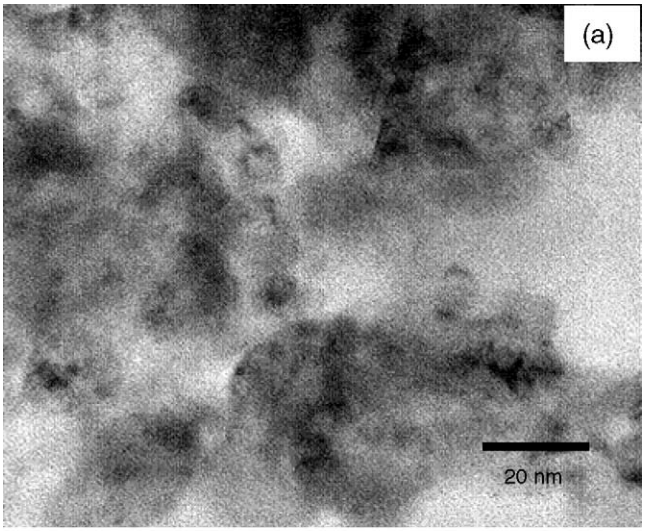

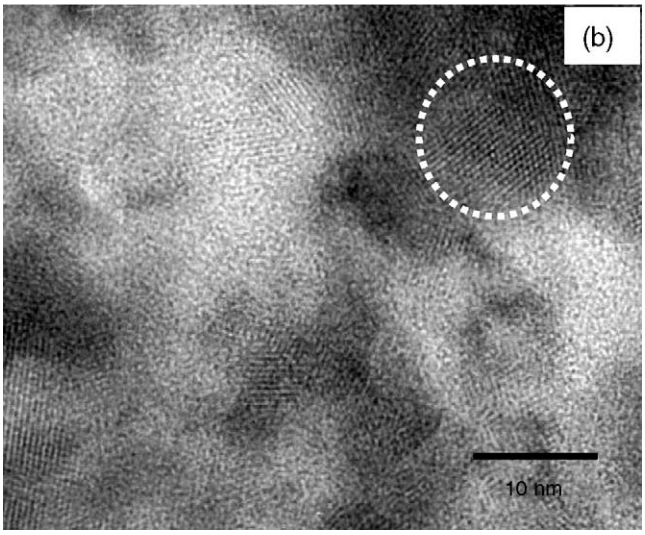

Fig. 5. Transmission electron micrograph of: (a) $LiNi_{0.5}Mn_{1.5}O_{3.95}S_{0.05}$ fired at 500 °C for 5 h; (b) high resolution micrograph for $LiNi_{0.5}Mn_{1.5}O_{3.95}S_{0.05}$.

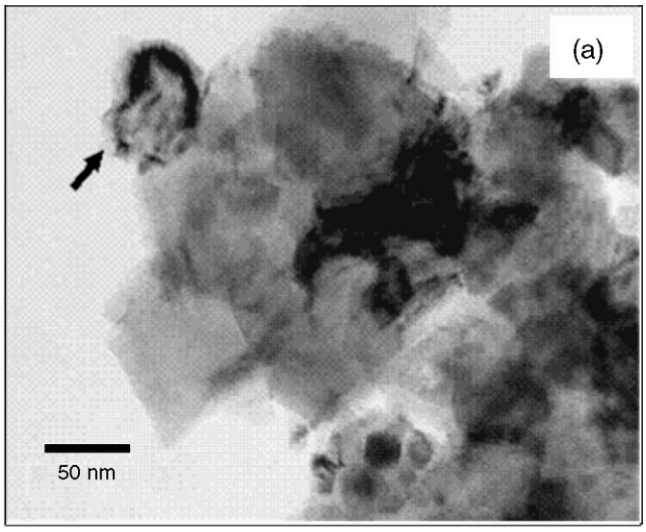

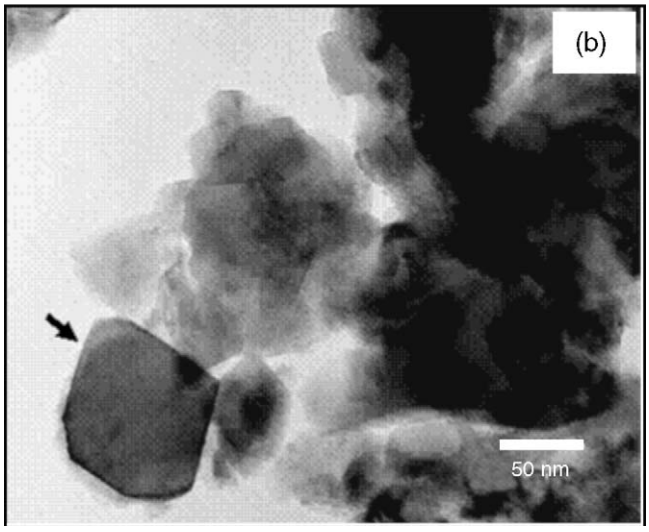

Fig. 7. Transmission electron micrograph of: (a) $LiNi_{0.5}Mn_{1.5}O_{3.95}S_{0.05}$ at 800 °C; (b) $LiNi_{0.5}Mn_{1.5}O_4$ at 800 °C.

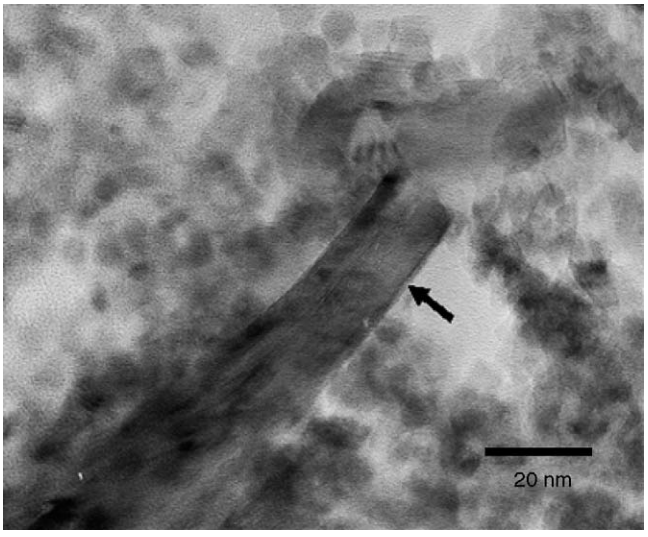

Fig. 6. Magnified transmission electron micrograph of sulfur-free $LiNi_{0.5}Mn_{1.5}O_4$ prepared at 500 °C for 5 h.

The reversible insertion–extraction of lithium in the 3-V reigon for $LiNi_{0.5}Mn_{1.5}O_{4-x}S_x$ ($x=0$ and 0.05) takes place topotactically in a solid matrix [25]. It has also been found [17] that $Li_1Ni_{0.5}Mn_{1.5}O_4$ has extra capacity (74 mA h g^{-1}) in the 2-V range that originates from extra lithium insertion into tetrahedral sites. Generally, the manganese spinel ($LiMn_2O_4$) exhibits rapid capacity fading in the 3 V range on account of severe volume changes that accompany transition from the cubic to the tetragonal phase [3,8,17]. This effect can be responsible for more than 50% of the capacity loss during the initial few cycles [2,9]. Unlike $Li_xMn_2O_4$, the $LiNi_{0.5}Mn_{1.5}O_{4-x}S_x$ ($x=0$ and 0.05) samples prepared at 500 °C do not show rapid capacity fading in the 3 V range. The samples do not contain Mn^{3+} ions, which are replaced by Ni^{2+} so that the oxidation state of manganese in the structure remains as 4+. The initial oxidation state of Mn in the formula $LiNi_{0.5}Mn_{1.5}O_4$ is +4 and changes to +3.3 when 1 mol of lithium is fully inserted into the structure. Theoretically, Jahn-Teller distortion should occur when ~0.75 mol of lithium are inserted into the structure to give rise to $Mn^{+3.5}$

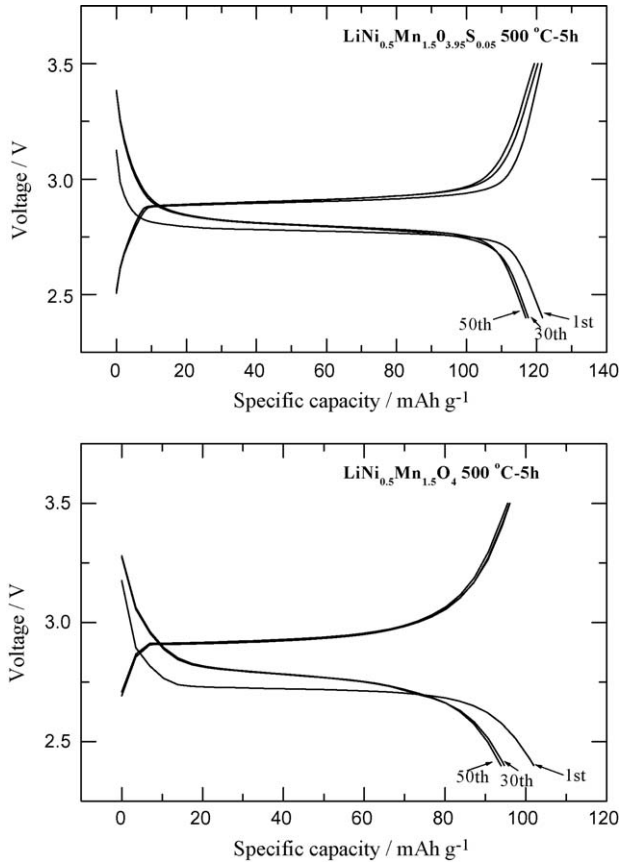

Fig. 8. Discharge–charge curves of Li/$LiNi_{0.5}Mn_{1.5}O_{4-x}S_x$ ($x = 0$ and 0.05) prepared at 500 °C for 5 h at current density of 0.2 mA cm^{-2}.

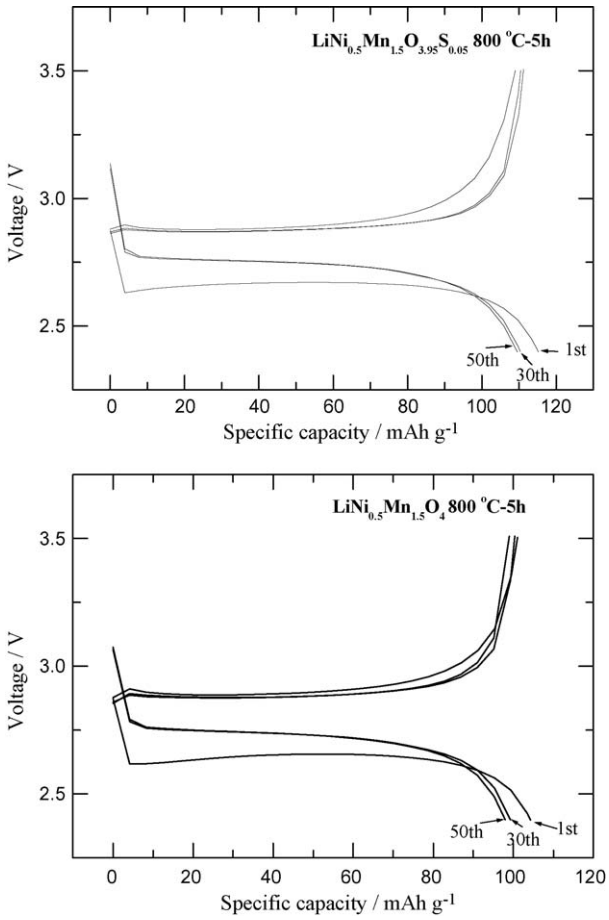

Fig. 9. Discharge–charge curves of Li/$LiNi_{0.5}Mn_{1.5}O_{4-x}S_x$ ($x = 0$ and 0.05) prepared at 800 °C for 5 h at current density of 0.2 mA cm^{-2}.

ions. Recently, we reported [27] the direct synthesis of nano-sized spinel $LiMn_2O_4$ powders with a particle size of 20 nm that exhibited no capacity loss in the 3-V region, even after 50 cycles. Although the nano-sized materials suffer from the Jahn-Teller distortion, that in turn give rises to a phase transition, the strain within the particles induced by the phase transition occurs in random directions. Therefore, the net deformation of a particle with nanograins is relieved by sliding at the grain boundaries, so that the total strain within the particles almost disappears. It is considered that the improved cycling behaviour is due to the formation of cathode particles with nano-scale primary grains of 10 nm that can withstand cubic-to-tetragonal phase transitions.

The cycling performance of $LiNi_{0.5}Mn_{1.5}O_{4-x}S_x$ ($x = 0$ and 0.05) prepared at 800 °C is presented in Fig. 9. Good capacity retention for both samples is observed over 50 cycles. The initial capacity of $LiNi_{0.5}Mn_{1.5}O_{3.95}S_{0.05}$ is 116 mA h g^{-1}, and up to 95% of this value is maintained even after 50 cycles. A comparison of the cycling performance of $LiNi_{0.5}Mn_{1.5}O_{4-x}S_x$ ($x = 0$ and 0.05) prepared different temperatures (500 and 800 °C) is given in Fig. 10. The sulfur-doped powder ($LiNi_{0.5}Mn_{1.5}O_{3.95}S_{0.05}$) prepared at 800 °C exhibits better capacity retention (95%) than $LiNi_{0.5}Mn_{1.5}O_4$ (93%). Sulfur-doped $LiNi_{0.5}Mn_{1.5}O_{3.95}S_{0.05}$ samples prepared at 500 and 800 °C deliver higher reversible capacities than those of sulfur-free $LiNi_{0.5}Mn_{1.5}O_4$.

The enhanced electrochemical behaviour of the sulfur-doped spinel ($LiNi_{0.5}Mn_{1.5}O_{3.95}S_{0.05}$) is attributed to the morphological features mentioned earlier, i.e., the rough morphology of the primary particles with smaller particle size is favourable in accommodating the internal stress associated with Jahn-Teller distortion during cycling. Goodenough et al. [13,26] previously reported that rapid capacity fading of spinel in the 3-V region could be improved by ball milling, which not only breaks up individual particles but also increases the surface roughness of each particle through numerous microscopic fractures. Based on the present work and reported studies [10,15], it is proposed that the subtle changes in the morphology of the primary particles caused by sulfur doping are partly responsible for the enhanced electrochemical performance of $LiNi_{0.5}Mn_{1.5}O_{3.95}S_{0.05}$.

The discharge capacities of $LiNi_{0.5}Mn_{1.5}O_{4-x}S_x$ ($x = 0$ and 0.05) compounds prepared at 500 °C are given in Fig. 11. The cell containing $LiNi_{0.5}Mn_{1.5}O_{3.95}S_{0.05}$ initially delivered 119 mA h g^{-1} at the *C*/5 rate. At higher cycling rates such as 5*C*, the cell still delivers quite an attractive capacity (72 mA h g^{-1}) in the cycled voltage range. A similar rate capability was observed for sulfur-free $LiNi_{0.5}Mn_{1.5}O_4$ but with lower reversible capacity. The good rate capability can be attributed to the smaller particle size, due to the suppression of parti-

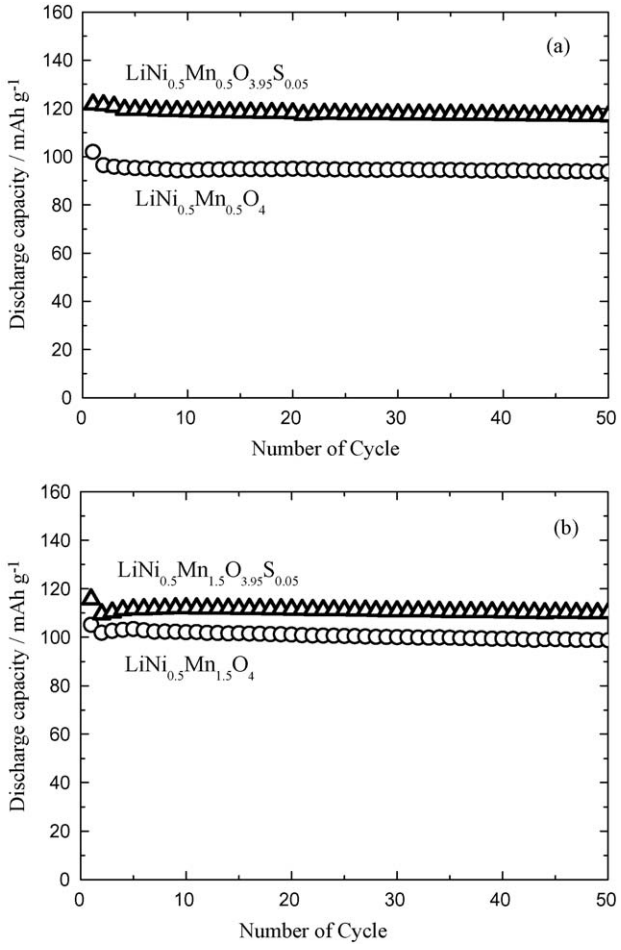

Fig. 10. Cycling performance of Li/$LiNi_{0.5}Mn_{1.5}O_{4-x}S_x$ ($x = 0$ and 0.05) prepared at: (a) 500 °C and (b) 800 °C for 5 h in voltage range of 2.4–3.5 V at current density of 0.2 mA cm^{-2}.

cle growth by sulfur doping. For smaller particles, the overall length for lithium diffusion is quite small and hence the insertion–extraction of lithium ions can be achieved in very short time intervals.

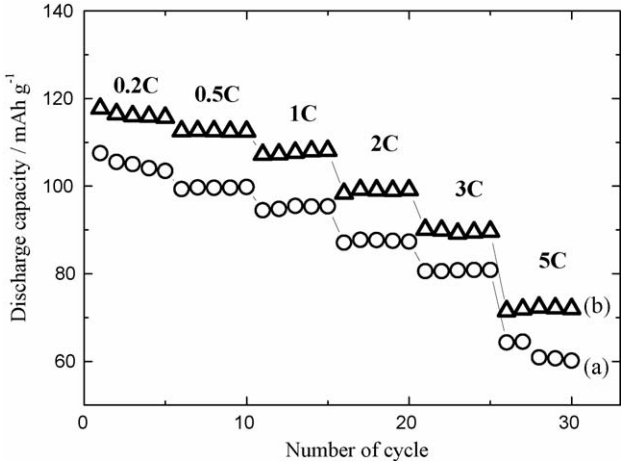

Fig. 11. Discharge capacity of: (a) Li/$LiNi_{0.5}Mn_{1.5}O_4$ and (b) Li/$LiNi_{0.5}Mn_{1.5}O_{3.95}S_{0.05}$ prepared at 500 °C in voltage range of 2.4–3.5 V at various current levels (1*C* assumed to be 148 mA h g^{-1}).

4. Conclusions

Spinel $LiNi_{0.5}Mn_{1.5}O_{4-x}S_x$ ($x = 0$ and 0.05) powders are synthesized by co-precipitation of different temperatures and using a carbonate precursor $(Ni_{0.5}Mn_{1.5})CO_3$. Powders prepared with sulfur doping at 500 and 800 °C have well-defined spinel structures. $LiNi_{0.5}Mn_{1.5}O_4$ (no-sulfur doping) shows an unknown XRD peak at $2\theta = 15$°C and contains impurities. The reversible capacity for both sulfur-doped and sulfur-free $LiNi_{0.5}Mn_{1.5}O_4$ are 121 and 102 mA h g^{-1}, respectively. $LiNi_{0.5}Mn_{1.5}O_{3.95}S_{0.05}$ prepared at 500 °C exhibits excellent capacity retention in the 3-V region and also good rate capability. Compared with sulfur-doped $LiNi_{0.5}Mn_{1.5}O_{3.95}S_{0.05}$, $LiNi_{0.5}Mn_{1.5}O_4$ delivers less reversible capacity in the tested voltage range. Scanning electron and transmission electron micrographs suggest that sulfur doping affects the morphological properties of $LiNi_{0.5}Mn_{1.5}O_4$. Doping of the spinel with sulfur produces morphological changes that appear to enhance the electrochemical performance of $LiNi_{0.5}Mn_{1.5}O_{3.95}S_{0.05}$ in terms of reversible capacity and cycling performance. The existence of sulfur in the prepared material is confirmed by chemical analysis (Sulfur analyzer, Leco, CS600, USA). The location of sulfur, i.e., in the surface or in the structure, is not clear at present and is the subject of further investigations.

Acknowledgement

This work was supported by the Core Technology Development Program of the Ministry of Commerce, Industry and Energy (MOCIE), Korea.

References

[1] G. Pistoia, G. Wang, C. Wang, Solid State Ionics 58 (1992) 285.
[2] J.M. Tarascon, E. Wang, F.K. Shokoohi, W.R. McKinnon, S. Colson, J. Electrochem. Soc. 138 (1991) 2859.
[3] G.G. Amatucci, J.M. Tarascon, J. Electrochem. Soc. 149 (2002) K31.
[4] Y. Xia, Y. Zhou, M. Yoshio, J. Electrochem. Soc. 144 (1997) 2593.
[5] G.G. Amatucci, N. Pereira, T. Zheng, J.M. Tarascon, J. Electrochem. Soc. 148 (2001) A171.
[6] Y.-K. Sun, Solid State Ionics 100 (1997) 115.
[7] K. Amine, H. Tukamoto, H. Yasuda, Y. Fujita, J. Electrochem. Soc. 143 (1996) 1607.
[8] P. Arora, B.N. Popov, R.E. White, J. Electrochem. Soc. 145 (1998) 807.
[9] Y. Ein-Eli, J.T. Vaughey, M.M. Thackeray, S. Mukerjee, X.Q. Yang, J. McBreen, J. Electrochem. Soc. 146 (1999) 908.
[10] Y.-K. Sun, Electrochem. Commun. 2 (2000) 6.
[11] H.J. Bang, V.S. Donepudi, J. Prakash, Electrochim. Acta 48 (2002) 443.
[12] Y.-K. Sun, G.-S. Park, Y.-S. Lee, M. Yoshio, K.S. Nahm, J. Electrochem. Soc. 148 (2001) A994.
[13] S.H. Kang, J.B. Goodenough, J. Electrochem. Soc. 147 (2000) 3621.
[14] M.M. Thackeray, Prog. Solid State Chem. 25 (1997) 1.
[15] Y.-K. Sun, Y.S. Jeon, H.J. Lee, Electrochem. Solid State Lett. 3 (2000) 7.
[16] J. Cho, M.M. Thackeray, J. Electrochem. Soc. 146 (1999) 3577.
[17] K. Ariyoshi, Y. Iwakoshi, N. Nakayama, T. Ohzuku, J. Electrochem. Soc. 151 (2004) A296.
[18] Q. Zhong, A. Bonakdarpour, M. Zhang, Y. Gao, J.R. Dahn, J. Electrochem. Soc. 144 (1997) 205.
[19] S.H. Park, S.W. Oh, S.-T. Myung, Y.-K. Sun, J. Electrochem. Solid State Lett. 151 (2004) A451.

[20] J.-H. Kim, S.-Y. Myung, C.S. Yoon, I.-H. Oh, Y.-K. Sun, J. Electrochem. Soc. 151 (2004) A1911.
[21] S.-H. Park, H.-S. Shin, S.-T. Myung, C.S. Yoon, K. Amine, Y.-K. Sun, Chem. Mater. 17 (2005) 6.
[22] H.-S. Shin, S.H. Park, Y.C. Bae, Y.-K. Sun, Solid State Ionics 176 (2005) 2577.
[23] J.M. Tarascon, E. Wang, F.K. Shokoohi, W.R. Mckinnon, S. Colson, J. Electrochem. Soc. 138 (1991) 2589.
[24] J.E. Huheey, Inorganic Chemistry, 3rd ed., Harper and Row Pub, New York, USA, 1983, pp. 73–76.
[25] T. Ohzuku, M. Kitagawa, T. Hirai, J. Electrochem. Soc. 137 (1990) 769.
[26] J.B. Goodenough, M.M. Thackeray, W.I.F. David, P.G. Bruce, Rev. Chim. Miner. 21 (1984) 435.
[27] S.-H. Park, S.-T. Myung, S.W. Oh, C.S. Yoon, Y.-K. Sun, Electrochim. Acta 51 (2006) 4089.